Chapter 9

Simplifying the Reconstruction Algorithm for the Refractive Index Decrement Using the Auxiliary Function $\tilde{\delta}$[1]

9.1 Introduction

Consider an experiment with an object illuminated by a plane monochromatic X-ray wave with wavelength λ and intensity I_{in} and with the transmitted wave registered by a position-sensitive detector. We only consider here the case of fully coherent X-rays, however, the theory can be extended to the partially-coherent case as in (Gureyev et al., 2004a; Myers et al., 2007b).

The main idea of this Chapter, the introduction of an auxiliary function to simplify the process of 3D reconstruction of the refractive index, is from Timur Gureyev, the principal results are obtained by the candidate herself under the supervision of Timur Gureyev and Konstantin Pavlov. The computer simulations are done by Thomas Baillie under the supervision of Timur Gureyev and Konstantin Pavlov.

9.2 Theoretical Background

The propagation direction of the incident X-ray wave, $\sqrt{I_{in}}e^{ikz'}$, makes an angle θ' with the z-axis in the xy-plane, where $-\pi/2 \leqslant \theta' < \pi/2$. It will be also convenient to use the angle $\theta = \theta' + \pi/2$ (Figure 9.1).

[1]This Chapter is based on a joint paper with Thomas Baillie, Timur Gureyev and Konstantin Pavlov (Baillie et al., 2012)

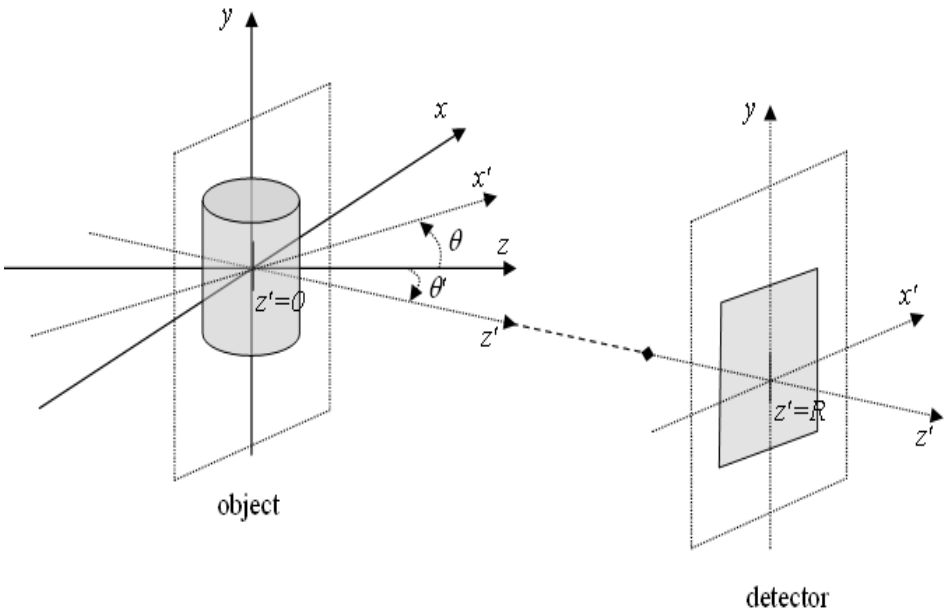

Figure 9.1: Generic layout of the in-line CT experimental setup.

We assume as usual that the projection approximation (Born and Wolf, 2005, Ch. 4.11) can be applied to calculate the phase and intensity, respectively, of the wave after transmission through the object (see Chapter 3),

$$\phi_\theta(x', y) = -k(P_\theta \delta)(x', y), \tag{9.1}$$

$$I_\theta(x', y) = I_{in} e^{-2k(P_\theta \beta)(x', y)}, \tag{9.2}$$

where P_θ is the projection operator (Equation (6.2)) and $\mathbf{r}' = (x', y, z')$ are Cartesian coordinates rotated by the angle θ' around the y axis with respect to coordinate system $\mathbf{r}$ (Figure 9.1). Note that we formally refer the transmitted intensity and phase distribution to the plane $z' = 0$, rather than the object plane located immediately downstream the object along the direction of propagation of the X-ray wave. As it will be seen below, this assumption is mathematically convenient and acceptable in the case of thin objects, i.e. those objects whose thickness is much smaller than the distance between the object and the X-ray detector.

In order to accomplish a reconstruction of the real part of the refractive

index in the object, related to the phase of the transmitted beam via Equation (9.1), one needs to have an accurate quantitative model relating the transmitted phase distribution, $\phi_\theta(x', y)$, to the in-line intensity in the image, $I_\theta^d(x', y)$, acquired at a free-propagation distance d from the object. One such model is given by the finite-difference form of the Transport of Intensity Equation (TIE) (Chapter 5), which can be written as follows:

$$I_\theta^d(x', y) = I_\theta(x', y) - \frac{d}{k} \nabla_\perp \cdot \left(I_\theta(x', y) \nabla_\perp \phi_\theta(x', y) \right). \tag{9.3}$$

Teague suggested to solve Equation (9.3) via the introduction of an auxiliary function ψ_θ (Chapter 8), which satisfies

$$\nabla_\perp \psi_\theta(x', y) = I_\theta(x', y) \nabla_\perp \phi_\theta(x', y). \tag{9.4}$$

As described in Chapter 8, if such a scalar potential ψ_θ exists, then a solution for the phase function in Equation (9.4) can be determined by solving two Poisson equations:

$$-\nabla_\perp^2 \psi_\theta(x', y) = \frac{k}{d} \left(I_\theta^d(x', y) - I_\theta(x', y) \right) \tag{9.5}$$

and

$$\nabla_\perp^2 \phi_\theta(x', y) = \nabla_\perp \cdot \left(I_\theta^{-1}(x', y) \nabla_\perp \psi_\theta(x', y) \right). \tag{9.6}$$

This approach provides a method for solving Equation (9.3) with respect to the unknown phase $\phi_\theta(x', y)$, if the intensity distributions $I_\theta(x', y)$ and $I_\theta^d(x', y)$ are known (Teague, 1983; Paganin and Nugent, 1998a). One advantage of this approach, compared to a direct numerical solution of Equation (9.3), is that the former is amenable to an implementation using the Fast Fourier transform (FFT). Note however, that the phase distribution reconstructed by means of two Poisson equations may in some special cases differ from an exact solution of Equation (9.3). This issue is discussed in detail in Chapter 8 (Schmalz et al., 2011).

After the phase distribution $\phi_\theta(x', y)$ is reconstructed at each projection angle θ, it is possible to reconstruct the 3D distribution of the real part of refractive index by CT techniques (Chapter 6). Taking the 2D Fourier transform of the projection $P_\theta(x', y)$ (Equation (6.2)) and using the Fourier slice theorem

(Equation (6.5)), (Natterer, 2001, Ch. II.2) we obtain that

$$f(x,y,z) = \int_0^{\pi}\int_{-\infty}^{\infty}\int_{-\infty}^{\infty} e^{2\pi i(\xi'(x\sin\theta+z\cos\theta)+y\eta)}\mathbf{F_2}[P_\theta f](\xi',\eta,\theta)|\xi'|d\xi' d\eta d\theta, \quad (9.7)$$

where $\mathbf{F_2}[P_\theta]$ is the 2D Fourier transform (Equation (A.3)). Note that in Chapter 6 we used a different definition of the angular parameters. Therefore, if projections $(P_\theta f)(x',y)$ can be measured for all view angles θ from the interval $[0,\pi)$, Equation (9.7) can be used to reconstruct the 3D distribution $f(x,y,z)$. Following this approach with respect to Equation (9.1), we obtain

$$\delta(x,y,z) = -\frac{1}{k}\int_0^{\pi}\int_{-\infty}^{\infty}\int_{-\infty}^{\infty} e^{2\pi i(\xi'(x\sin\theta+z\cos\theta)+y\eta)}\mathbf{F_2}[\phi_\theta](\xi',\eta)|\xi'|d\xi' d\eta d\theta, \quad (9.8)$$

where $\phi_\theta(x',y)$ can be computed at each angle θ by means of the Poisson Equations (9.5) and (9.6). Note that in the case of Equation (9.2) the same approach yields the conventional (absorption) CT reconstruction formula:

$$\beta(x,y,z) = -\frac{1}{2k}\int_0^{\pi}\int_{-\infty}^{\infty}\int_{-\infty}^{\infty} e^{2\pi i(\xi'(x\sin\theta+z\cos\theta)+y\eta)}\mathbf{F_2}\left[\ln\left(\frac{I_\theta}{I_{in}}\right)\right](\xi',\eta)|\xi'|d\xi' d\eta d\theta. \quad (9.9)$$

One can see that Equation (9.9) provides a single-step reconstruction algorithm for the quantity of interest, $\beta(x,y,z)$, from a measurable quantity, $I_\theta(x',y)$. On the other hand, Equation (9.8) requires a preliminary step of phase reconstruction from measurable quantities, $I_\theta(x',y)$ and $I^d_\theta(x',y)$ at each view angle. Apart from additional computational complexity, the two-step reconstruction of the real part of refractive index suffers from well-known numerical instabilities (Bronnikov, 1999; Gureyev et al., 2006): one associated with the low spatial frequencies in the Poisson Equation (9.5) and the other one due to the (moderatefication in Equation (9.7) of high-frequency noise due to the effect of the ramp filter (multiplication by $|\xi'|$ in Fourier space).

These problems can be partially eliminated in the case of objects with negligible absorption, by means of a single-step reconstruction formula due to

Bronnikov (Bronnikov, 1999):

$$\delta(x,y,z) = \\ -\frac{1}{4\pi^2 d}\int_0^{\pi}\int_{-\infty}^{\infty}\int_{-\infty}^{\infty} e^{2\pi i(\xi'(x\sin\theta+z\cos\theta)+\eta y)}\frac{|\xi'|}{\xi'^2+\eta^2}\mathcal{F}_2\left[\ln\left(\frac{I_\theta^d}{I_{in}}\right)\right](\xi',\eta)d\xi' d\eta d\theta. \tag{9.10}$$

Equation (9.10) can be obtained by substitution into Equation (9.8) of a simplified form of the TIE solution

$$\phi_\theta(x',y) = -\frac{k}{d}\nabla_\perp^{-2}\left(\frac{I_\theta^d}{I_{in}}-1\right), \tag{9.11}$$

which one gets from the Poisson Equations (9.5) and (9.6) in the case $I_\theta(x',y) \approx I_{in}$, and using the (optional) approximation $1-I_\theta^d(x',y)/I_{in} \approx -\ln(I_\theta^d(x',y)/I_{in})$, which holds under the general validity conditions of the TIE (Chapter 8). Note that Equation (9.10) not only provides a single-step reconstruction algorithm for the decrement of the refractive index, $\delta(x,y,z)$, but also partially eliminates the above mentioned instabilities of the reconstruction thanks to the cancellation of the noise-amplification effect of the ramp filter $|\xi'|$ by the Fourier-space kernel of the Laplace operator, $\frac{1}{\xi'^2+\eta^2}$.

A similar (but much stronger) stabilisation of the PCT reconstruction with respect to noise in the input data is achieved in the case of homogeneous objects (Paganin et al., 2004a; Gureyev et al., 2006). The latter class of objects includes objects consisting predominantly of a single material, and, in the case of X-rays with energies between approximately $60keV$ and $500keV$, any objects containing only light chemical elements with $Z < 10$ (Wu et al., 2005).

Using Equation (9.10) one can easily verify the following identity:

$$\nabla^2\delta(x,y,z) = \frac{1}{d}\int_0^{\pi}\int_{-\infty}^{\infty}\int_{-\infty}^{\infty} e^{2\pi i(\xi'(x\sin\theta+z\cos\theta)+\eta y)}\mathcal{F}_2\left[\ln\left(\frac{I_\theta^d}{I_{in}}\right)\right](\xi',\eta)|\xi'|d\xi' d\eta d\theta, \tag{9.12}$$

where we used the identity

$$\nabla^2 e^{2\pi i(\xi'(x\sin\theta+z\cos\theta)+\eta y)} = -4\pi^2(\xi'^2+\eta^2)e^{2\pi i(\xi'(x\sin\theta+z\cos\theta)+\eta y)} \tag{9.13}$$

in the derivation. This can be viewed as a form of commutativity of the Laplace operator and the Radon transform (Natterer, 2001, Ch. II.1), (Cloetens et al.,

1997b), see the proof in Appendix (Lemma (E.3)). This property is also directly related to the commonality between the eigenfunctions of the Laplace operator in a circle and the singular functions of the Radon transform (Myers et al., 2007a).

Using Equation (9.12), the single-step reconstruction algorithm, Equation (9.10), can be re-written in the following form:

$$\delta(x,y,z) = \frac{1}{d}\nabla^{-2}\left[\int_0^{\pi}\int_{-\infty}^{\infty}\int_{-\infty}^{\infty} e^{2\pi i(\xi'(x\sin\theta+z\cos\theta)+\eta y)}\mathbf{F_2}\left[\ln\left(\frac{I_\theta^d}{I_{in}}\right)\right](\xi',\eta)|\xi'|d\xi' d\eta d\theta\right]. \tag{9.14}$$

In Equation (9.14) the phase retrieval step (inverse Laplacian) takes place in 3D after the conventional CT reconstruction. This approach could present an advantage in the case of general objects, where the phase retrieval in 2D involves the subtraction of two projection images collected at different object-to-detector distances (see e.g. Equation (9.5)). Indeed, as explained above, such subtraction often involves substantial practical problems, as it is strongly affected by the changes in the illumination conditions with time (i.e. by the temporal fluctuations of low spatial frequencies of the incident beam). One can expect that certain types of random background fluctuations will average out in the process of image summation during CT reconstruction (at the backprojection step). Moreover, some misalignment issues, such as e.g. disagreement between angular positions of the sample at different object-to-detector distances, become largely irrelevant after the CT reconstruction. Of course, systematic variations in the background illumination during CT scans will still affect the phase retrieval in 3D, but these variations may arguably be also easier to track and correct during or after the CT reconstruction (note that the mutual alignment of two 3D distributions is likely to be more efficient compared to pair-wise correlations of projections).

Unfortunately, in the cases with non-trivial absorption the approach which led to Equation (9.14) is usually no longer valid, as, unlike the Laplace operator, the general TIE operator, $D_{TIE}[\phi_\theta](x',y) = -\nabla_\perp \cdot (I_\theta(x',y)\nabla_\perp\phi_\theta(x',y))$, does not commute with the Radon transform. This is why we propose the following

approach based on the Teague's method for solution of the TIE described above.

9.3 Definition of an Auxiliary Function $\tilde{\delta}$

Let us assume that there exists a function $\tilde{\delta}(x, y, z)$ such that

$$\psi_\theta(x', y) = -kI_{in}(P_\theta\tilde{\delta})(x', y), \tag{9.15}$$

where the function $\psi_\theta(x', y)$ is defined by Equation (9.4). Then, according to Equation (9.5) and Equation (9.7), we obtain

$$\tilde{\delta}(x, y, z) = -\frac{1}{4\pi^2 d}\int_0^\pi\int_{-\infty}^{\infty}\int_{-\infty}^{\infty} e^{2\pi i(\xi'(x\sin\theta+z\cos\theta)+\eta y)}\frac{|\xi'|}{\xi'^2+\eta^2}F_2\left[\frac{I_\theta^d - I_\theta}{I_{in}}\right]d\xi' d\eta d\theta. \tag{9.16}$$

Therefore, the 3D distribution of the quantity $\tilde{\delta}(x, y, z)$ can be obtained by a single-step CT reconstruction algorithm from the transmitted intensity distributions measured at two different object-to-detector distances for each view angle.

By an exact analogy with the derivation of Equation (9.14) from Equation (9.10), one can now also derive the following reconstruction formula from Equation (9.16):

$$\tilde{\delta}(x, y, z) = \frac{1}{d}\nabla^{-2}\left(\int_0^\pi\int_{-\infty}^{\infty}\int_{-\infty}^{\infty} e^{2\pi i(\xi'(x\sin\theta+z\cos\theta)+\eta y)}|\xi'|F_2\left[\frac{I_\theta^d}{I_{in}}\right]d\xi' d\eta d\theta - \int_0^\pi\int_{-\infty}^{\infty}\int_{-\infty}^{\infty} e^{2\pi i(\xi'(x\sin\theta+z\cos\theta)+\eta y)}|\xi'|F_2\left[\frac{I_\theta}{I_{in}}\right]d\xi' d\eta d\theta\right). \tag{9.17}$$

Thus, unlike the function $\delta(x, y, z)$, the new quantity $\tilde{\delta}(x, y, z)$ can be computed by applying the 3D inverse Laplacian to the difference between the two conventional CT reconstructions (only without the logarithm operation) obtained from projections collected at different object-to-detector distances. Note that

in experiments the incident intensity I_{in} corresponding to the measurements of $I_\theta(x', y)$ and $I^d_\theta(x', y)$ can be different, which can be easily taken into account in Equation (9.17).

9.4 Physical Nature of the Auxiliary Function $\tilde{\delta}(x, y, z)$

An important question that needs to be answered with respect to quantity $\tilde{\delta}(x, y, z)$ is that about its physical nature. Firstly, we note that in the case of objects with negligible absorption, i.e. when it is possible to use the approximation $I_\theta(x', y) \approx I_{in}$, Equation (9.16) reduces to Equation (9.10), and hence $\tilde{\delta}(x, y, z) \equiv \delta(x, y, z)$ in this case. In the general case, when absorption inside the object cannot be ignored, the quantity $\tilde{\delta}(x, y, z)$ depends both on the real and imaginary parts of the complex refractive index. The following formal expression can be derived from Equations (9.16), (9.5), (9.3), (9.1) and (9.2):

$$\tilde{\delta}(x, y, z) = -\frac{1}{4\pi^2} \int_0^\pi \int_{-\infty}^{\infty} \int_{-\infty}^{\infty} e^{2\pi i(\xi'(x\sin\theta + z\cos\theta) + \eta y)} \frac{|\xi'|}{\xi'^2 + \eta^2} \times F_2 \left[\nabla_\perp \cdot \left(e^{-2k P_\theta \beta(x', y)} \nabla_\perp (P_\theta \delta)(x', y) \right) \right] d\xi' d\eta d\theta. \quad (9.18)$$

Equation (9.18) establishes an explicit relationship between the introduced quantity $\tilde{\delta}(x, y, z)$ and the complex refractive index. It also shows that the quantity $\tilde{\delta}(x, y, z)$ always exists and is unique as long as the complex refractive index is amenable to the mathematical operations involved in Equation (9.18). However, as far as the physical nature of the quantity is concerned, Equation (9.18)) does not appear particularly helpful, rather than demonstrating again that in the case of negligible absorption, when $e^{-2k(P_\theta \beta)(x', y)} \approx 1$, one gets $\tilde{\delta}(x, y, z) \equiv \delta(x, y, z)$. To obtain a simplified relationship between $\tilde{\delta}(x, y, z)$ and the complex refractive index, we assume that all projections of the imaginary part of the refractive index, $\beta(x, y, z)$, are slowly varying functions with respect to all their arguments. Then we can apply the divergence operator to both parts of Equation (9.4) and move the gradient operator out of the brackets

(neglecting the terms that contain derivatives of $e^{-2k(P_\theta\beta)(x',y)}$):

$$\nabla_\perp^2(P_\theta\tilde{\delta})(x', y) = \nabla_\perp \cdot \left(e^{-2k(P_\theta\beta)(x',y)}\nabla_\perp(P_\theta\delta)(x', y)\right) \approx \nabla_\perp^2\left(e^{-2k(P_\theta\beta)(x',y)}(P_\theta\delta)(x', y)\right). \quad (9.19)$$

Hence, assuming e.g. the Dirichlet boundary conditions, we conclude from Equation (9.19) that $(P_\theta\tilde{\delta})(x', y) = e^{-2k(P_\theta\beta)(x',y)}(P_\theta\delta)(x', y)$ due to the uniqueness of the solution to the boundary value problem for the Laplace equation. Using again the assumption about the slow variation of $(P_\theta\beta)(x', y)$ (this time with respect to variables x' and θ), we can now obtain:

$$(P_\theta\tilde{\delta})(x', y) \approx e^{-2k\langle P\beta\rangle(y)}(P_\theta\delta)(x', y) = P_\theta\left(e^{-2k\langle P\beta\rangle(y)}\delta\right)(x', y), \quad (9.20)$$

where $\langle\ \rangle$ denotes averaging over x' and θ, and the y variable here plays the role of a free parameter which does not affect any operations in the xz-plane. As a complete set of parallel projections over 180 degrees uniquely defines a 2D distribution, this allows one to obtain the following equation:

$$\delta(x, y, z) \approx \tilde{\delta}(x, y, z)e^{2k\langle P\beta\rangle(y)}. \quad (9.21)$$

Equation (9.21) can be used to find the approximate values of the real part of the decrement of refractive index, $\delta(x, y, z)$, from the recovered distributions of $\tilde{\delta}(x, y, z)$ and $\beta(x, y, z)$.

We carried out computer experiments with numerically simulated objects (phantoms) that generate different amounts of X-ray absorption and refraction at a given X-ray energy in order to investigate the behavior of the quantity $\tilde{\delta}(x, y, z)$ as a function of the real and imaginary parts of the refractive index of the phantoms. The results of the simulations presented in the next section of the chapter shed some light on the nature of physical information about the object that can be obtained by means of in-line phase-contrast CT experiments combined with the simplified reconstruction algorithm described by Equation (9.16) or Equation (9.17). The simple formula (Equation (9.21)) connecting $\tilde{\delta}$, δ and β for certain type of objects was also verified by our simulations.

9.5 Methods and Results

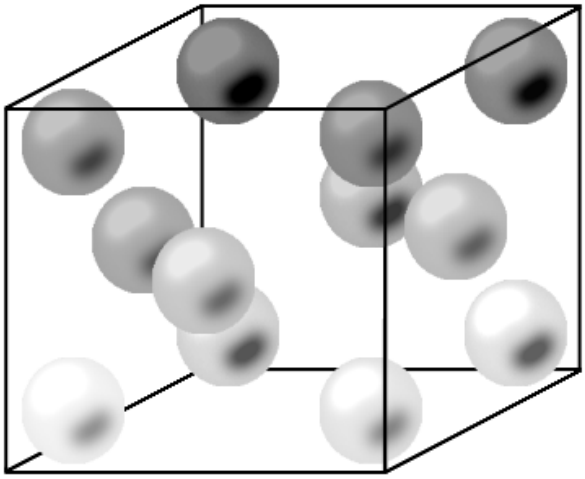

Figure 9.2: The structure of the simulated object. It consisted of twelve spheres arranged in three layers of four, each parallel to the base. The bottom and top layers had the spheres situated in the corners, and the middle layer had them in the centre of each face. The lightness of the spheres decreases with increasing β for the constant δ objects, δ for the constant β objects, and β and δ for the objects with both varying. The β and δ of the background matrix are zero.

The simulated object, as depicted in Figure 9.2, was a collection of 12 non-overlapping homogeneous spheres of radius 100 μm, one in each of the eight corners of the bounding cube and one on each face excluding the top and bottom. It was represented as two $1024 \times 1024 \times 1024$ arrays of 32-bit floating-point numbers, corresponding to the β and δ distributions of the complex refractive index $n = 1 - \delta + i\beta$, which was different for each of the spheres. The β and δ of the background matrix are zero. Both arrays were stored and processed as 1024 square planar cross sections parallel to the xz-plane. The voxel size was $1 \times 1 \times 1 \mu m^3$.

The simulations were performed using X-TRACT (X-TRACT, 2010, Site accessed June 2012), a program that amongst other things allows one to

calculate parallel-beam X-ray projections of objects given the object's β and δ slices. X-TRACT allows one to perform a variety of useful image operations such as pixel-wise addition and inverse Laplacian, to process image files into sinograms, and to perform CT reconstructions by calculating the inverse Radon transform of sinogram images. All of these operations were required for the simulations.

First, X-TRACT was used to generate parallel-beam projections of the object at two different sample-to-detector propagation distances, namely $0\,\mathrm{cm}$ and $10\,\mathrm{cm}$. These projections were simulated for the X-ray wavelength of 1 Å. A Gaussian filter with the width $2\sigma = 4$ pixels was applied to each stack of slices before propagating. This models sharpness of the interfaces of the object and the implicit convolutions with point-spread functions of the source and the detector. In total, 180 of these projections were generated, with each projection corresponding to a one degree rotation of the object from the previous position.

The derivative of the intensity in the direction of propagation, $\partial_z I_\theta(x', y)$ was then approximated by performing a pixelwise subtraction of the $10\,\mathrm{cm}$ projection from the $0\mathrm{cm}$ projection and then dividing by the propagation distance, i.e $10\,\mathrm{cm}$. Next an inverse 2D Laplacian operation was performed on each derivative image, and because the boundary conditions make the inverse Laplacian unique only up to an additive constant, this constant was approximated—by averaging the background values—and subtracted in order to force the background values to be as close to zero as possible. The images were also multiplied by the quantity $-k/d$ in order to generate the 2D distributions of the function $\psi_\theta(x', y)$ in accordance with Equation (9.5). The obtained images were then used to create a series of sinograms from projections $\psi_\theta(x', y)$, and the CT reconstruction was performed to these sinograms in the same way as normally applied for the solution of Equation (9.1). This process yielded the 3D distribution of the quantity $\tilde{\delta}(x, y, z)$ in accordance with Equation (9.15).

In order to explore the relationship between the complex refractive index $n = 1-\delta+i\beta$ and $\tilde{\delta}$ with regards to CT reconstruction, six different objects were used: three with constant δ and three with constant β. Then, to more closely model experimental results, the constant β simulations were performed again with Poisson noise being added to the projections, with a relative standard deviation, σ_{rel}, of 5% calculated for the average intensity.

The three constant β objects had β values of 1.5×10^{-9}, 1×10^{-8}, and 2×10^{-8}, each with a δ range of 5×10^{-8} to 1×10^{-6}. The three constant δ objects had δ values of 5×10^{-7}, 1×10^{-6}, and 2×10^{-6}, each with a β range of 1×10^{-9} to 2×10^{-8}. These values were chosen close to refractive indices of certain real materials; at a wavelength of 1 Å (X-ray complex refraction coefficients, 2012, Site accessed June 2012) are shown in Table 9.1. The results are shown in

Material	δ	β
Perspex	1.7216×10^{-6}	1.6736×10^{-9}
Nylon	1.6743×10^{-6}	1.3706×10^{-9}
SiO_2	3.3790×10^{-6}	1.9517×10^{-8}
Brain	1.5549×10^{-6}	2.3889×10^{-9}
Adipose	1.3955×10^{-6}	1.2362×10^{-9}

Table 9.1: Components of refractive indices of certain real materials at a wavelength of 1 Å

Figures 9.3, 9.4 and 9.5, and all confirmed the theoretical prediction that $\tilde{\delta}$ would approach δ as β approached 0.

Figure 9.3 suggests that $\tilde{\delta}$ can be approximated by a linear function $\tilde{\delta} = m\delta$, with $0 < m < 1$, in agreement with Equation (9.21) for constant β. This is also supported by Figure 9.5, and both Figures show the curves of best fit for each simulation's data series. Tables 9.2 and 9.3 show the values of $\frac{\langle P\beta \rangle}{\beta}$ corresponding to each curve of best fit.

Figure 9.5 also demonstrates that Equation (9.21) may allow one to accurately obtain the function $\delta(x, y, z)$ from the reconstructed functions $\tilde{\delta}(x, y, z)$ and $\beta(x, y, z)$ in the cases with significant spatial variation of both β and δ/β.

For comparison, we have also performed the reconstruction of the real decrement of the refractive index $\delta(x, y, z)$ in the sample with constant $\beta = 1.5 \times 10^{-9}$ using the PCT reconstruction formulæ for homogeneous objects (Gureyev et al., 2006) with $\delta = 5 \times 10^{7}$ (which approximately corresponded to an average δ value for this sample). The appropriate results are shown in Figure 9.3 by green triangular symbols. These data demonstrate that the "homogeneous" TIE method, although producing reasonable looking CT reconstructions, cannot quantitatively reconstruct with satisfying accuracy the distribution of the real decrement of the refractive index in objects with significant spatial variability

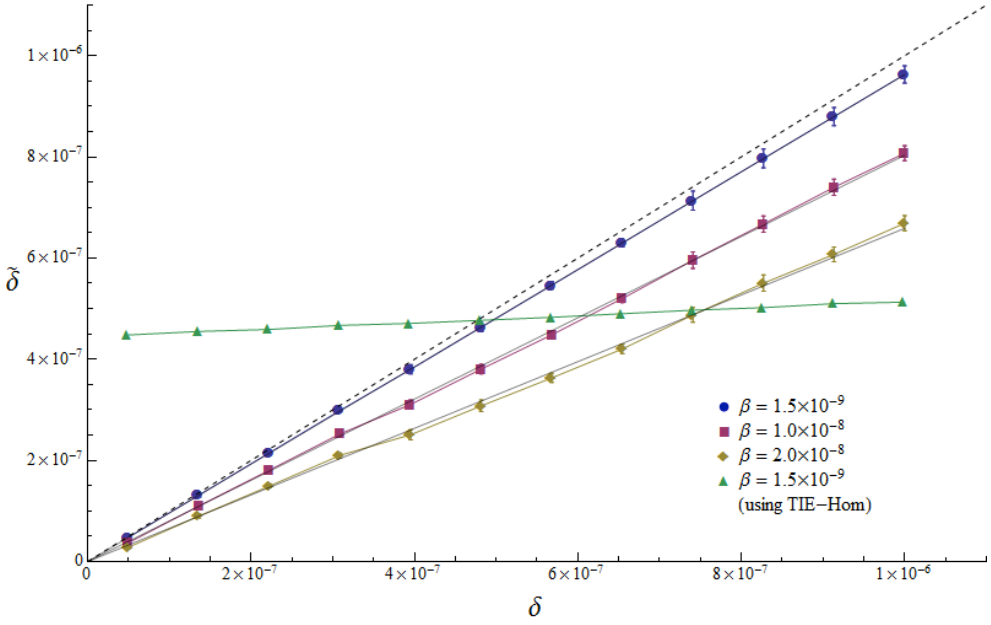

Figure 9.3: The reconstructed values using $\tilde{\delta}$ for the three objects with constant β (closed circles, squares and diamond symbols). The dashed line is $\tilde{\delta} = \delta$. The uncertainty is taken to be 1 standard deviation of the values in the centre of the spheres in the reconstructed slices. Also shown are the curves of best fit $\tilde{\delta} = \delta e^{-2k\frac{\langle P\beta\rangle}{\beta}\beta}$ for closed circles, squares and diamond symbols, with the parameters shown in Table 9.2. The triangular symbols show the result of a "homogenous" TIE reconstruction.

of the ratio.

β	$\frac{\langle P\beta\rangle}{\beta}(\mu m)$
1.5×10^{-9}	201
1.0×10^{-8}	174
2.0×10^{-8}	166

Table 9.2: The best-fit parameters used in Figures 9.3 and 9.4.

Figure 9.4 shows the constant β reconstructions with 5% noise. Whilst being visibly more unstable than their noiseless counterparts, the quantity $\tilde{\delta}(x, y, z)$ is still reconstructed with remarkable stability and closely followed the same trend lines.

The graphs of Figure 9.5, whilst being largely linear, are all marred by a small but systematic 'jump' between the fourth and fifth data points. This jump is likely caused by the geometry of the simulated object, as the four

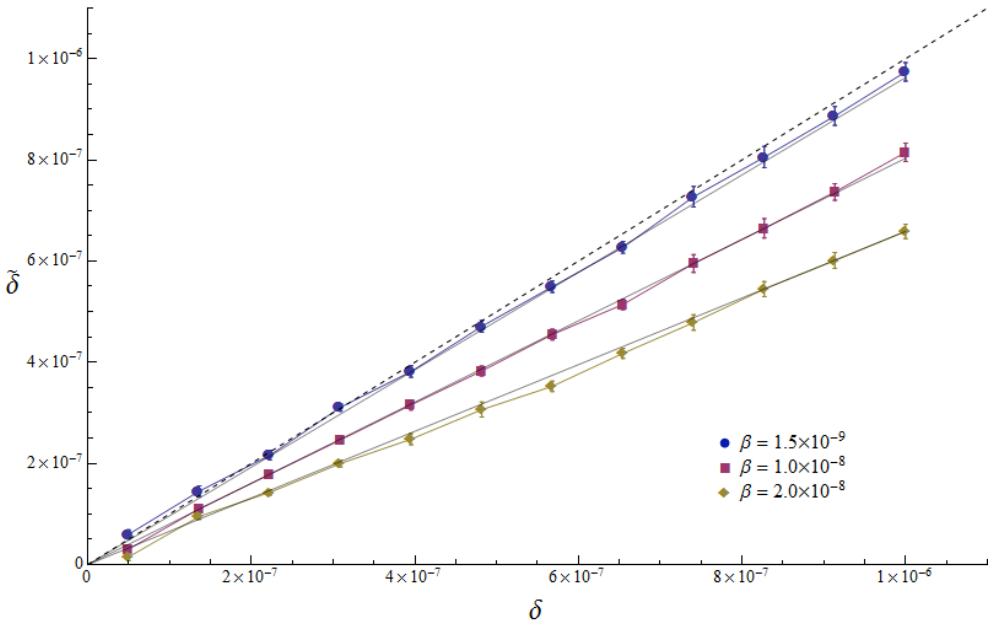

Figure 9.4: The reconstructed values using $\tilde{\delta}$ for the three objects with constant β and 5% Poisson noise. The dashed line is $\tilde{\delta} = \delta$. The uncertainty is taken to be 1 standard deviation of the values in the centre of the spheres in the reconstructed slices. Also shown are the same curves of best fit as in Figure 9.3.

spheres in the middle layer are closer together than those in the top and bottom layers.

δ	$\frac{\langle P\beta \rangle}{\beta}(\mu m)$
5×10^{-7}	160
1.0×10^{-6}	161
2.0×10^{-6}	162

Table 9.3: The best-fit parameters used in Figure 9.5.

Figure 9.6 shows the projection at $\theta = 26^{o}$ of the object with $\delta = 5 \times 10^{-7}$ at an object-to-detector propagation distance of 10cm, along with a cross-section through the bottom layer of spheres. Visible are the bright diffraction fringes encircling each sphere, as typical for the in-line phase-contrast images.

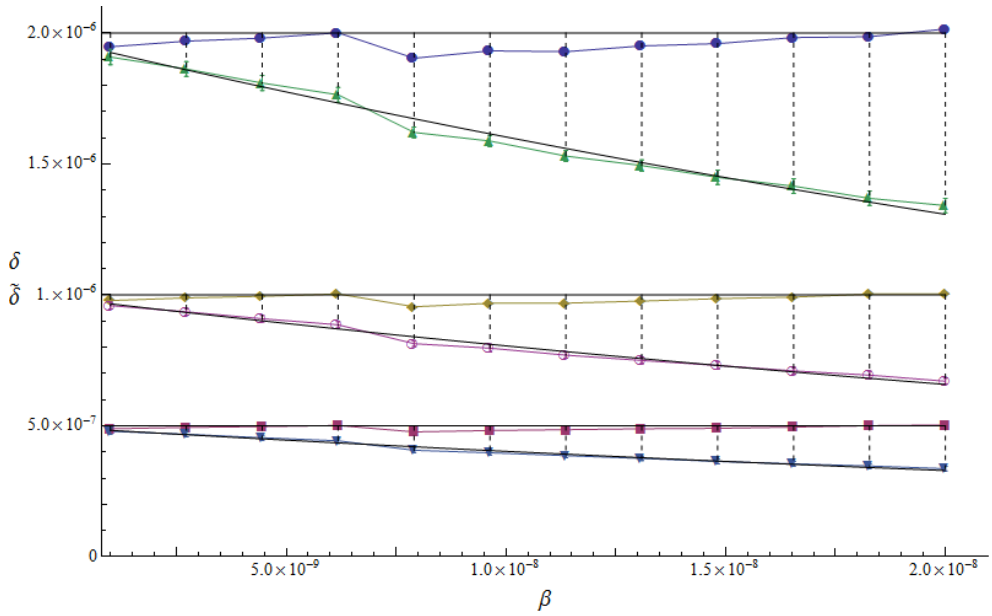

Figure 9.5: $\tilde{\delta}$ (triangular, open circles and inverted triangular symbols) and the reconstructed values of δ (see Equation (9.21)) (closed circles, diamond and square symbols) using $\tilde{\delta}$ for the three objects with constant δ. The uncertainty is taken to be 1 standard deviation of the values in the centre of the spheres in the reconstructed slices. Also shown are the curves of best fit $\tilde{\delta} = \delta e^{-2k\frac{\langle P\beta\rangle}{\beta}\beta}$, which parameters are given in Table 9.3.

9.6 Summary

We presented a variant of in-line phase-contrast tomography based on the Teague's method. Our newly introduced quantity $\tilde{\delta}(x, y, z)$ is uniquely related to the complex refractive index in the object and can be reconstructed using two projections at different propagation distances collected at each view angle. We argue that this approach may present certain advantages compared to the more conventional PCT approach that requires phase retrieval to be applied at each projection angle separately. Furthermore, knowing the distributions of $\tilde{\delta}$ and β in the object, may allow one to find the real decrement of the refractive index, δ of materials in the object. Namely, we showed that for a certain class of objects the connection between $\tilde{\delta}$, δ and β can be approximated by a simple expression, $\delta \approx \tilde{\delta}(x, y, z)e^{2k\langle P\beta\rangle(y)}$, where $\langle P\beta\rangle(y)$ is the projection $(P_\theta\beta)(x', y)$ averaged over the coordinates x' and θ. Our computer simulations have shown that this significantly simplified reconstruction procedure is stable with respect

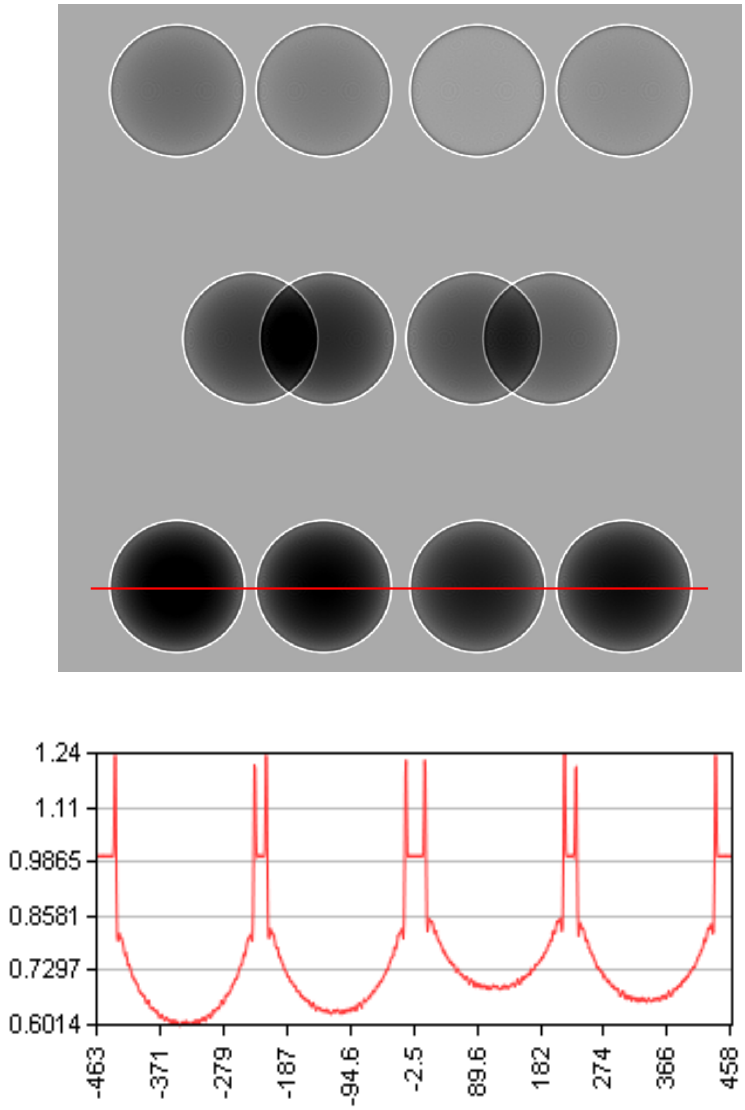

Figure 9.6: Typical projection with an object-to-detector propagation distance of 10 cm and a cross section indicated by the solid line through the bottom row of spheres.

to noise.

Chapter 10

Conclusions

We present results obtained by the candidate in collaboration with her co-authors.

10.1 Green's Functions

Chapter 7 presented a general method for finding the fundamental solution of the Helmholtz equation, i.e. function $G(x, y, z)$ satisfying the equation

$$(\nabla^2 + k^2)G(x, y, z) = -4\pi\delta(x, y, z), \tag{10.1}$$

subject to Sommerfeld radiation conditions (Equation 7.3).

This method differs from other established methods (Section 7.5). While other established methods find three particular solutions (which happen to be an incoming, an outgoing and an standing wave), one of which (the outgoing wave) satisfies the Sommerfeld radiation condition, the method used here first finds all possible fundamental solutions, namely

$$\hat{G} = \nu.p.\frac{1}{\pi(\xi^2 + \eta^2 + \zeta^2 - \rho^2)} + \mu\delta_S, \tag{10.2}$$

where $\mu\delta_S$ is a simple layer on the sphere S with μ, see Equation (7.14).

We then choose the solution satisfying the Sommerfeld radiation condition:

$$G(r) = \frac{e^{ikr}}{r}, \tag{10.3}$$

where $r = \sqrt{x^2 + y^2 + z^2}$.

The Helmholtz equation is the basis for our subsequent results, as the TIE (Section 5.2) was derived from the paraxial form of the Helmholtz equation.

10.2 Teague's Method

Conditions for the validity of Teague's method for solving the TIE were studied in Chapter 8. The problem is that this technique uses the substitution of $I\nabla_\perp\phi$ by $\nabla_\perp\psi$, which exists only if ψ is a scalar potential for $I\nabla_\perp\phi$. We show that this substitution is an exact one only if either the vectors $\nabla_\perp I(x,y)$ and $\nabla_\perp\phi(x,y)$ are parallel to each other at each point (x,y) of the simply connected domain Ω, or at least one of the vectors is zero. The condition that the vectors $\nabla_\perp I(x,y)$ and $\nabla_\perp\phi(x,y)$ are parallel to each other holds for a class of objects, including homogeneous objects, the condition $\nabla_\perp I(x,y)=0$ holds for phase objects, and the case $\nabla_\perp\phi(x,y)=0$ is not of interest for the phase retrieval problem.

A sufficient condition for the validity of Teague's method in the case of generic objects is that

$$\frac{kL_\Omega^3}{R}\|\nabla_\perp \ln I\|_2 \leqslant \|\phi\|_2, \tag{10.4}$$

where L_Ω is the diameter of the domain, R is the distance between the object and the image planes, and $\|\ \|_2$ is the L_2-norm as defined in Equation (8.23).

While these conditions are usually satisfied in practice, we provided an example (Chapter 8.6), for which the L_2-norm of the difference between the exact solution, $\phi(x,y)$, and solution obtained by Teague's method, $\tilde{\phi}(x,y)$, is approximately nine percent of the norm of the exact solution: $\|\phi(x,y)-\tilde{\phi}(x,y)\|_2 \approx 0.09\|\phi(x,y)\|_2$. This shows that it would be useful to verify that the conditions above are satisfied, before using the phase-retrieval technique based on the Teague's method for solving the TIE.

10.3 The Auxiliary Function $\tilde{\delta}$

Chapter 9 applied Teague's method to 3D imaging. We introduced an auxiliary function, $\tilde{\delta}(x,y,z)$ (Section 9.15), whose projection (Equation (6.2)) along each irradiation direction given by an angle θ, is proportional to the function $\psi_\theta(x',y)$, for which Teague's proposed substitution ($\nabla_\perp\psi_\theta = I_\theta\nabla_\perp\phi_\theta$) is valid:

$$(P_\theta\tilde{\delta})(x',y) = -\frac{1}{kI_{in}}\psi_\theta(x',y). \tag{10.5}$$

Here I_{in} is the X-ray's intensity before the interaction with the object, $I_\theta(x', y)$ and $\phi_\theta(x', y)$ are the X-ray intensity and the phase distributions over the object plane (x', y), after the interaction of X-rays with the object, for a corresponding angle θ. This newly introduced auxiliary function $\tilde{\delta}(x, y, z)$ contains some information about the real and imaginary parts of the refractive index.

We derived the formula for the single-step reconstruction of the function $\tilde{\delta}(x, y, z)$ directly from the intensity measurements, without the intermediate step of phase retrieval for each angle θ:

$$\tilde{\delta}(x, y, z) = \\ -\frac{1}{4\pi^2 d I_{in}} \int_0^{\pi} \int_{-\infty}^{\infty} \int_{-\infty}^{\infty} e^{2\pi i(\xi'(x\sin\theta + z\cos\theta) + \eta y)} \frac{|\xi'|}{\xi'^2 + \eta^2} F_2 \left[I_\theta^d - I_\theta \right] d\xi' d\eta d\theta. \tag{10.6}$$

Here I_θ^d is the intensity distribution over the image plane, and d is the distance between the object and the image planes.

The first advantage of the single-step method over the two-steps method is that the calculations become simpler.

A second advantage arises because, while Equation (10.6) is similar to the formula for the absorption index distribution retrieval (Equation (9.9)), which is used in conventional CT, the difference is significant in that in Equation (10.6) the ramp filter $|\xi'|$ is divided by $\xi'^2 + \eta^2$. This leads to better stability, as high frequency noise is scaled by $\frac{|\xi'|}{\xi'^2+\eta^2}$, which tends to zero as $|\xi'| \to \infty$.

We established the relationship between the auxiliary function $\tilde{\delta}(x, y, z)$ and the refractive index decrement distribution $\delta(x, y, z)$ (Section 9.4):

$$\tilde{\delta}(x, y, z) = \\ -\frac{1}{4\pi^2} \int_0^{\pi} \int_{-\infty}^{\infty} \int_{-\infty}^{\infty} e^{2\pi i(\xi'(x\sin\theta + z\cos\theta) + \eta y)} \frac{|\xi'|}{\xi'^2 + \eta^2} \times \\ F_2 \left[\nabla_\perp \cdot \left(e^{-2k P_\theta \beta(x', y)} \nabla_\perp (P_\theta \delta)(x', y) \right) \right] d\xi' d\eta d\theta. \tag{10.7}$$

This is the precise relation between the functions $\delta(x, y, z)$ and $\tilde{\delta}(x, y, z)$, but the physical meaning of the function $\tilde{\delta}(x, y, z)$ is not entirely clear. We can see from Equation (10.7) that the functions $\delta(x, y, z)$ and $\tilde{\delta}(x, y, z)$ coincide for

phase objects ($\beta \approx 0$). In the case that all projections of $\beta(x, y, z)$ are slowly varying functions, Equation (10.7) can be reduced to a simple form:

$$\delta(x, y, z) \approx \tilde{\delta}(x, y, z) e^{2k\langle P\beta\rangle(y)}, \tag{10.8}$$

where $\langle\ \rangle$ is an average over x' and θ. Computer simulations (Section 9.5) support the latter formula.

10.4 Future Applications

The result of Chapter 7 clarifies the process of finding the Green's function for the Helmholtz equation. This formalism, which uses generalised functions, can be applied in quantum mechanics, as the time-independent Schrödinger equation has the same form as the Helmholtz equation. More generally, this approach can be used for solving boundary value problems for partial differential equations in physics and engineering.

The result of Chapter 8 can be applied in the phase-contrast imaging to verify the validity of Teague's method for solving the TIE. This result is relevant to phase retrieval in quantitative phase-contrast imaging using electrons, neutrons and matter waves.

In Chapter 9 Teague's method is applied to tomography. This approach provides a simplified and stabilised way for reconstruction of 3D distribution of refractive index in optically opaque samples. This can be useful in many areas of science and technology, for example, in materials and life sciences.

Bibliography

Acosta, G. and Duran, R. G. (2004). An optimal Poincaré inequality in for convex domains. *Proceedings of the American Mathematical Society*, 132:195. (Cited on page 73.)

Aharonov, Y. and Bohm, D. (1961). Further considerations on electromagnetic potentials in the quantum theory. *Physical Review Letters*, 123:1511–1524. (Cited on page 8.)

Allman, B. E., McMahon, P. J., Nugent, K. A., Paganin, D., Jacobson, D. L., Arif, M., and Werner, S. A. (2000). Imaging: Phase radiography with neutrons. *Nature*, 408:158–159. (Cited on pages 7, 8, 9, 43, 65 and 79.)

Als-Nielsen, J. and McMorrow, D. (2001). *Elements of Modern X-Ray Physics*. John Wiley & Sons Sons. (Cited on pages 21, 22 and 23.)

Anastasio, M. A., Shi, D., De Carlo, F., and Pan, X. (2004). Analytic image reconstruction in local phase-contrast tomography. *Physics in Medicine and Biology*, 49:121–144. (Cited on page 50.)

Authier, A. (2005). *Dynamical Theory of X-Ray Diffraction*. Oxford University Press, New York. (Cited on page 16.)

Baillie, T. W., Gureyev, T. E., Schmalz, J. A., and Pavlov, K. M. (2012). Phase-contrast X-ray tomography using Teague's method. *Opt. Express*, 20(15):16913–16925. Available from: `http://www.opticsexpress.org/abstract.cfm?URI=oe-20-15-16913`. (Cited on pages 10, 13 and 81.)

Bajt, S., Barty, A., Nugent, K. A., McCartney, M., Wall, M., and Paganin, D. (2000). Quantitative phase-sensitive imaging in a transmission electron microscope. *Ultramicroscopy*, 83:67–73. (Cited on pages 6, 7, 8, 9, 43, 65 and 79.)

Barrett, H. H. and Meyers, K. J. (2004). *Foundation of Image Science*. Wiley-Interscience. (Not cited.)

Barty, A., Nugent, K. A., D., P., and Roberts, A. (1998). Quantitative optical phase microscopy. *Optics Letters*, 23:817–819. (Cited on pages 6, 8, 9, 43, 65 and 79.)

Barty, A., Nugent, K. A., Roberts, A., and Paganin, D. M. (2000). Quantitative phase tomography. *Opt. Commun.*, 175(4):329–336. (Cited on page 50.)

Beltran, M. A., Paganin, D. M., Uesugi, K., and Kitchen, M. J. (2010). 2D and 3D X-ray phase retrieval of multi-material objects using a single defocus distance. *Opt. Express*, 18(7):6423–6436. Available from: http://www.opticsexpress.org/abstract.cfm?URI=oe-18-7-6423. (Cited on page 11.)

Bonse, U. and Busch, F. (1996). X-ray computed microtomography (μCT) using synchrotron radiation (SR). *Progress in Biophysics and Molecular Biology*, 65(1–2):133–169. Available from: http://www.sciencedirect.com/science/article/pii/S0079610796000119, doi:http://dx.doi.org/10.1016/S0079-6107(96)00011-9. (Cited on page 9.)

Bonse, U. and Hart, M. (1965). An X-ray interferometer. *Applied Physics Letters*, 6:155. (Cited on page 25.)

Born, M. and Wolf, E. (2005). *Principles of Optics*. Cambridge University Press, London. (Cited on pages 10, 11, 14, 17, 35, 36, 52 and 82.)

Bravin, A. (2003). Exploiting the x-ray refraction contrast with an analyzer: the state of the art. *J. Phys. D Appl. Phys.*, 36:A24–A29. (Cited on page 30.)

Bremmer, H. (1952). On the asymptotic evaluation of diffraction integrals with a special view to the theory of defocusing and optical contrast. *Physica*, 18:469–485. (Cited on page 8.)

Bronnikov, A. V. (1999). Reconstruction formulas in phase-contrast tomography. *Optics Communications*, 171(4-6):239. Available from: http://adsabs.harvard.edu/abs/1999OptCo.171..239B. (Cited on pages 11, 12, 84 and 85.)

Bronnikov, A. V. (2002). Theory of quantitative phase-contrast computed tomography. *J. Opt. Soc. Am. A*, 19(3):472–480. (Cited on page 11.)

Bruning, J. H., Herriott, D. R., Gallagher, J. E., Rosenfeld, D. P., White, A. D., and Brangaccio, D. J. (1974). Digital wavefront measuring interferometer for testing optical surfaces and lenses. *Appl. Opt.*, 13(11):2693–2703. Available from: http://ao.osa.org/abstract.cfm?URI=ao-13-11-2693. (Cited on page 27.)

Bushuev, V. A., Ingal, V. N., and Beliaevskaya, E. A. (1998). Wave theory of X-ray phase-contrast radiography. *Chrystallography Reports*, 43(4):538–547. (Cited on page 30.)

Chapman, D., Thomlinson, W., Johnston, R., Washburn, D., Pisano, E., Gmür, N., Zhong, Z., Menk, R. H., Arfelli, F., and Sayers, D. (1997). Diffraction enhanced x-ray imaging. *Phys. Med. Biol*, 42(11):2015–2025. (Cited on page 32.)

Cloetens, P. (2011). Private communication. (Cited on page 72.)

Cloetens, P., Guigay, J. P., De Martino, C., Baruchel, J., and Schlenker, M. (1997a). Fractional Talbot imaging of phase gratings with hard x-rays. *Opt. Lett.*, 22(14):1059–1061. Available from: http://ol.osa.org/abstract.cfm?URI=ol-22-14-1059. (Cited on page 34.)

Cloetens, P., Ludwig, W., Baruchel, J., Van Dyck, D., Van Landuyt, J., Guigay, J. P., and Schlenker, M. (1999). Holotomography: Quantitative phase tomography with micrometer resolution using hard synchrotron radiation x rays. *Applied Physics Letters*, 75(19):2912–2914. Available from: http://scitation.aip.org/content/aip/journal/apl/75/19/10.1063/1.125225. (Cited on page 36.)

Cloetens, P., Pateyron-Salome, M., Buffiere, J. Y., Peix, G., Baruchel, J., Peyrin, F., and Schlenker, M. (1997b). Observation of microstructure and damage in materials by phase sensitive radiography and tomography. *Journal of Applied Physics*, 81(9):5878–5886. Available from: http://dx.doi.org/10.1063/1.364374. (Cited on pages 9, 11, 50 and 85.)

Cowley, J. M. (1995). *Diffraction Physics*. North-Holland, Amsterdam, 3rd edition. (Cited on page 8.)

Davydov, A. S. (1973). *Quantum Mechanics*. Nauka, Moscow. (Cited on pages 14, 52 and 59.)

De Caro, L., Cedola, A., Giannini, C., Bukreeva, I., and Lagomarsino, S. (2008). In-line phase-contrast imaging for strong absorbing objects. *Physics in Medicine and Biology*, 53(22):6619. Available from: http://stacks.iop.org/0031-9155/53/i=22/a=021. (Cited on pages 71 and 72.)

De Graef, M. and Zhu, Y. (2001). Quantitative noninterferometric Lorentz microscopy. *Journal of Applied Physics*, 89(11):7177–7179. Available from: http://dx.doi.org/10.1063/1.1355337. (Cited on pages 9, 43, 65 and 79.)

des Plantes, B. G. Z. (1932). Eine neue Methode zur Differenzierung in der Röntgenographie. *Acta Radiol.*, 13:182–192. (Cited on page 44.)

Diemoz, P. C., Coan, P., Glaser, C., and Bravin, A. (2010). Absorption, refraction and scattering in analyzer-based imaging: comparison of different algorithms. *Opt. Express*, 18(4):3494–3509. Available from: http://www.opticsexpress.org/abstract.cfm?URI=oe-18-4-3494. (Cited on page 32.)

Dilmanian, F. A., Zhong, Z., Ren, B., Wu, X. Y., Chapman, L. D., Orion, I., and Thomlinson, W. C. (2000). Computed tomography of x-ray index of refraction using the diffraction enhanced imaging method. *Phys. Med. Biol*, 45(4):933–946. (Cited on page 50.)

Dobbins, I. J. T. and Godfrey, D. J. (2003). Digital x-ray tomosynthesis: current state of the art and clinical potential. *Physics in Medicine and Biology*, 48:R65–R106. (Cited on pages 44 and 45.)

Evans, L. C. (1998). *Partial Differential Equations*. American Mathematical Society, Providence. (Cited on pages 67, 68, 69, 71 and 72.)

Fienup, J. R. (1993). Phase-retrieval algorithms for a complicated optical system. *Appl. Opt.*, 32(10):1737–1746. Available from: http://ao.osa.org/abstract.cfm?URI=ao-32-10-1737. (Cited on page 37.)

Fitzgerald, R. (2000). Phase-sensitive x-ray imaging. *Physics Today*, 53:23. (Cited on page 8.)

Frank, J., Altmeyer, S., and Wernicke, G. (2010). Non-interferometric, non-iterative phase retrieval by Green's functions. *J. Opt. Soc. Am. A*, 27(10):2244–2251. Available from: http://josaa.osa.org/abstract.cfm?URI=josaa-27-10-2244. (Cited on pages 43, 65 and 79.)

Garrison, J. B., Grant, D. G., Guier, W. H., and Johns, R. J. (1969). Three dimensional roentgenography. *Am. J. Roentgenol.*, 105:903–8. (Cited on page 44.)

Gbur, G. and Wolf, W. (2002). Diffraction tomography without phase information. *Opt. Lett.*, 27:1890–1892. (Cited on page 11.)

Gerchberg, W. and Saxton, W. O. (1972). A practical algorithm for the determination of the phase from image and diffraction plane pictures optik 35, 237 (1972). *Optik*, 35:237. (Cited on page 37.)

Ghiglia, D. C., Mastin, G. A., and Romero, L. A. (1987). Cellular-automata method for phase unwrapping. *J. Opt. Soc. Am. A*, 4(1):267–280. Available from: http://josaa.osa.org/abstract.cfm?URI=josaa-4-1-267. (Cited on page 29.)

Gierloff, J. J. (1987). Phase unwrapping by regions. *in Current Developments in Optical Engineering II SPIE*, 818:2–9. (Cited on page 29.)

Goldshtein, H. (1980). *Classical Mechanics*. Addison-Wesley, Singapore. (Cited on page 123.)

Goldstein, R. M., Zebker, H. A., and Werner, C. L. (1988). Satellite radar interferometry: Two-dimensional phase unwrapping. *Radio Science*, 23(4):713–720. Available from: http://dx.doi.org/10.1029/RS023i004p00713, doi:10.1029/RS023i004p00713. (Cited on page 29.)

Goodman, J. W. (2005). *Introduction to Fourier Optics*. Roberts &Company. (Cited on pages 37 and 49.)

Graef, M. D. (2003). *Introduction to Conventional Transmission Electron Microscopy*. Cambridge University Press, Cambridge. (Cited on page 63.)

Green, H. and Wolf, E. (1953). A scalar representation of the electromagnetic field. *Proc.Phys.Soc.*, A(66):1129–1137. (Not cited.)

Guigay, J. P. (1977). Fourier transform analysis of Fresnel diffraction patters and in-line holograms. *Opik*, 49(1):121–125. (Cited on page 41.)

Guigay, J. P., Langer, M., Boistel, R., and Cloetens, P. (2007). Mixed tranfer function and transport-of-intensity approach for phase retrieval in the Fresnel region. *Optic Letters*, 32:1617–1619. (Cited on pages 36 and 41.)

Guinier, A. (1963). *X-ray Diffraction*. W. H. Freeman and Company. (Cited on page 21.)

Gureyev, T. E. (2003). Composite techniques for phase retrieval in the fresnel region. *Opt. Commun.*, 220:49–58. (Cited on page 43.)

Gureyev, T. E., Mayo, S., Wilkins, S., Paganin, D., and Stevenson, A. W. (2001). Quantitative in-line phase-contrast imaging with multienergy X-rays. *Physical Review Letters*, 18;86(25):5827–30. (Cited on page 36.)

Gureyev, T. E., Mayo, S. C., Myers, D. E., Nesterets, Y., Paganin, D. M., Pogany, A., Stevenson, A. W., and Wilkins, S. W. (2009). Refracting Röntgen's rays: Propagation-based x-ray phase contrast for biomedical imaging. *Journal of Applied Physics*, 105(10):102005–12. Available from: http://dx.doi.org/10.1063/1.3115402. (Cited on pages 8 and 9.)

Gureyev, T. E. and Nugent, K. A. (1996). Phase retrieval with the transport-of-intensity equation. ii. orthogonal series solution for nonuniform illumination. *J. Opt. Soc. Am. A*, 13(8):1670–1682. Available from: http://josaa.osa.org/abstract.cfm?URI=josaa-13-8-1670. (Cited on page 42.)

Gureyev, T. E., Paganin, D. M., Myers, G. R., Nesterets, Y. I., and Wilkins, S. W. (2006). Phase-and-amplitude computer tomography. *Applied Physics Letters*, 89:034102. (Cited on pages 11, 84, 85 and 92.)

Gureyev, T. E., Paganin, D. M., Stevenson, A. W., Mayo, S. C., and Wilkins, S. W. (2004a). Generalized eikonal of partially coherent beams and its use in quantitative imaging. *Physical Review Letters*, 93(6):068103. (Cited on page 81.)

Gureyev, T. E., Pogany, A., Paganin, D. M., and Wilkins, S. W. (2004b). Linear algorithms for phase retrieval in the Fresnel region. *Optics Communications*, 231(1–6):53–70. Available from: http://www.sciencedirect.com/science/article/pii/S0030401803023320, doi:http://dx.doi.org/10.1016/j.optcom.2003.12.020. (Cited on pages 36 and 73.)

Gureyev, T. E., Raven, C., Snigirev, A., Snigireva, I., and Wilkins, S. W. (1999). Hard x-ray quantitative non-interferometric phase-contrast microscopy. *Journal of Physics D: Applied Physics*, 32(5):563. Available from: http://stacks.iop.org/0022-3727/32/i=5/a=010. (Cited on pages 9, 65 and 80.)

Gureyev, T. E., Roberts, A., and Nugent, K. A. (1995). Phase retrieval with the transport-of-intensity equation: matrix solution with use of Zernike polynomials. *J. Opt. Soc. Am. A*, 12(9):1932–1942. Available from: http://josaa.osa.org/abstract.cfm?URI=josaa-12-9-1932. (Cited on pages 42 and 65.)

Gureyev, T. E. and Wilkins, S. W. (1997). Regimes of X-ray phase-contrast imaging with perfect crystals. *Il Nuovo Cimento*, 19 D:545–552. (Cited on page 32.)

Gureyev, T. E. and Wilkins, S. W. (1998). On X-ray phase imaging with a point source. *Optical Society of America*, 15(3):579–585. (Cited on pages 8, 11 and 73.)

Harding, G., Kosanetzky, J. M., and Neitzel, U. (1985). Elastic scatter computed tomography. *Phys. Med. Biol.*, 30(2):183–186. (Cited on page 11.)

Helfen, L., Baumbach, T., Cloetens, P., and Baruchel, J. (2009). Phase-contrast and holographic computed laminography. *Applied Physics Letters*, 94:104103. (Cited on page 45.)

Helfen, L., Baumbach, T., Mikulik, P., Kiel, D., Pernot, P., Cloetens, P., and Baruchel, J. (2005). High-resolution three-dimensional imaging of flat objects by synchrotron-radiation computed laminography. *Applied Physics Letters*, 86:071915–1 – 071915–3. (Cited on page 45.)

Helfen, L., Myagotin, A., Rack, A., Pernot, P., Mikulik, P., Michiel, M. D., and Baumbach, T. (2007). Synchrotron-radiation computed laminography for high-resolution three-dimensional imaging of flat devices. *Physica Status Solidi*, 204(8):2760–2765. doi:DOI10.1002/pssa.200775676. (Cited on page 45.)

Henke, B., Gullikson, E., and Davis, J. (1993). X-ray interactions: photoabsorption, scattering, transmission, and reflection at e=50-30000 ev, z=1-92. *Atomic Data and Nuclear Data Tables*, 54(2):181–342. Available from: http://henke.lbl.gov/optical_constants/. (Cited on page 74.)

Herman, G. T. (1980). *Image Reconstruction from Projections. The Fundamentals of Computerized Tomography*. Academic Press. (Cited on page 10.)

Hörmander, L. (1958). On the division of distributions by polynomials. *Arkiv för matematik*, 3(53):554–568. (Cited on pages 52 and 55.)

Hu, C., Zhang, L., Li, H., and Lo, S. (2008). Comparison of refraction information extraction methods in diffraction enhanced imaging. *Opt Express*, 16(21):16704–16710. (Cited on page 33.)

Huang, C. and Nevels, D. (1992). A closed-form multidimensional free-space Green's function by the path-integral method. *Microwave and optical technology letters*, 5(5):225–227. (Cited on page 52.)

Huang, Z., Kang, K., and Yang, Y. (2007). Extraction methods of phase information for X-ray diffraction enhanced imaging. *Nuclear Instruments and Methods in Physics Research Section A*, 579(1):218–222. (Cited on pages 32 and 33.)

Huntley, J. M. and Saldner, H. (1993). Temporal phase-unwrapping algorithm for automated interferogram analysis. *Appl. Opt.*, 32(17):3047–3052. Available

from: http://ao.osa.org/abstract.cfm?URI=ao-32-17-3047. (Cited on page 29.)

Jackson, J. D. (1998). *Classical Electrodynamics*. John Wiley & Sons. (Cited on pages 14 and 52.)

Judge, T. R. and Bryanston-Cross, P. J. (1994). A review of phase unwrapping techniques in fringe analysis. *Optics and Lasers in Engineering*, 21(4):199–239. Available from: http://www.sciencedirect.com/science/article/pii/0143816694900736, doi:http://dx.doi.org/10.1016/0143-8166(94)90073-6. (Cited on page 29.)

Kak, A. C. and Slaney, M. (1999). *Principles of Computerized Tomographic Imaging*. IEEE Press, New-York. (Cited on pages 42, 47, 48, 49 and 57.)

Kivshar, Y. and Agrawal, G. P. (2003). *Optical Solitons: From Fibers to Photonic Crystals*. Academic Press, Amsterdam. (Cited on page 63.)

Lade, S. J., Paganin, D., and Morgan, M. J. (2005a). 3-D vector tomography of Doppler-transformed fields by filtered-backprojection. *Optics Communications*, 253(4–6):382–391. Available from: http://www.sciencedirect.com/science/article/pii/S0030401805004189, doi:http://dx.doi.org/10.1016/j.optcom.2005.04.070. (Cited on pages 9, 43 and 65.)

Lade, S. J., Paganin, D., and Morgan, M. J. (2005b). Electron tomography of electromagnetic fields, potentials and sources. *Optics Communications*, 253(4–6):392–400. Available from: http://www.sciencedirect.com/science/article/pii/S0030401805004190, doi:http://dx.doi.org/10.1016/j.optcom.2005.04.071. (Cited on pages 9, 43 and 65.)

Lang, S. (1987). *Linear Algebra*. Springer, New York. (Cited on page 55.)

Langer, M., Cloetens, P., Guigay, J.-P., and Peyrin, F. (2008). Quantitative comparison of direct phase retrieval algorithms in in-line phase tomography. *Medical Physics*, 35(10):4556–4566. Available from: http://dx.doi.org/10.1118/1.2975224. (Cited on pages 43, 65 and 79.)

Langer, M., Cloetens, P., and Peyrin, F. (2010). Regularization of phase retrieval with phase-attenuation duality prior for 3D holotomography. *IEEE Trans. Image Process.*, 19(9):2428–2436. (Cited on page 11.)

Laperle, C. M., Wintermeyer, P., Wands, J. R., Shi, D., Anastasio, M. A., Li, X., Ahr, B., Diebold, G. J., and Rose-Petruck, C. (2007). Propagation based differential phase contrast imaging and tomography of murine tissue with a laser plasma x-ray source. *Applied Physics Letters*, 91(17):173901–3. Available from: http://dx.doi.org/10.1063/1.2802728. (Cited on page 9.)

Lewis, R. A. (2004). Medical phase contrast x-ray imaging: current status and future prospects. *Physics in Medicine and Biology*, 49(16). (Cited on page 8.)

Madelung, E. (1927). Quantentheorie in hydrodynamischer Form. *Zeitschrift für Physik*, 40:322–326. (Cited on page 63.)

Maksimenko, A. (2007). Nonlinear extension of the x-ray diffraction enhanced imaging. *Applied Physics Letters*, 90(15):154106–3. Available from: http://dx.doi.org/10.1063/1.2721378. (Cited on page 33.)

Martin, A. V. and Allen, L. J. (2007). Measuring the phase of a Bose-Einstein condensate. *Physical Review A*, 76(5):053606. Available from: http://link.aps.org/doi/10.1103/PhysRevA.76.053606. (Cited on page 9.)

Mayo, S., Davis, T., Gureyev, T., Miller, P., Paganin, D., Pogany, A., Stevenson, A., and Wilkins, S. (2003). X-ray phase-contrast microscopy and microtomography. *Opt. Express*, 11(19):2289–2302. Available from: http://www.opticsexpress.org/abstract.cfm?URI=oe-11-19-2289. (Cited on pages 9 and 50.)

McMahon, P. J., Peele, A. G., Paterson, D., Lin, J. J. A., Irving, T. H. K., McNulty, I., and Nugent, K. A. (2003). Quantitative x-ray phase tomography with sub-micron resolution. *Optics Communications*, 217(1–6):53–58. Available from: http://www.sciencedirect.com/science/article/pii/S0030401802022812, doi:http://dx.doi.org/10.1016/S0030-4018(02)02281-2. (Cited on pages 43, 65 and 79.)

Merzbacher, E. (1961). *Quantum Mechanics*. John Wiley & Sons New York. (Cited on pages 14, 52 and 59.)

Messiah, A. (1999). *Quantum Mechanics*. Dover Publications, New York. (Cited on pages 14 and 52.)

Miller, E. R., McCurry, E. M., and Hruska, B. (1971). An infinite number of laminagrams from a infiite number of radiograph. *Radiology*, 98:249–55. (Cited on page 45.)

Momose, A., Kawamoto, S., Koyama, I., Hamaishi, Y., Takai, K., and Suzuki, Y. (2003). Demonstration of X-Ray Talbot interferometry. *Japanese Journal of Applied Physics*, 42(Part 2, No. 7B):L866–L868. (Cited on page 35.)

Momose, A., Takeda, T., and Itai, Y. (1995). X-ray computed tomography for observing biological specimens and organic materials. *Rev. Sci. Instrum.*, 66:1434–1436. (Cited on pages 9 and 50.)

Momose, A., Yashiro, W., Taked, a. Y., Suzuki, Y., and Hattori, T. (2006). Phase tomography by X-ray Talbot interferometry for biological imaging. *Jpn. J. Appl. Phys.*, 45(6A):5254–5262. (Cited on page 50.)

Morse, P. M. and Feshbach, H. (1953). *Methods of Theoretical Physics*. McGraw-Hill, New York. (Cited on pages 14 and 52.)

Myers, G. R., Gureyev, T. E., and Paganin, D. M. (2007a). Stability of phase-contrast tomography. *J. Opt. Soc. Am. A*, 24(9):2516–2526. Available from: http://josaa.osa.org/abstract.cfm?URI=josaa-24-9-2516. (Cited on page 86.)

Myers, G. R., Mayo, S. C., Gureyev, T. E., Paganin, D. M., and Wilkins, S. W. (2007b). Polychromatic cone-beam phase-contrast tomography. *Physical Review A*, 76(4):045804. (Cited on page 81.)

Natterer, F. (2001). *The Mathematics of Computerized Tomography*. SIAM, Philadelphia. (Cited on pages 10, 46, 47, 49, 84, 85 and 123.)

Nesterets, Y. I., Gureyev, T. E., Paganin, D., Pavlov, K. M., and Wilkins, S. W. (2004). Quantitative diffraction-enhanced x-ray imaging of weak

objects. *Journal of Physics D: Applied Physics*, 37(8):1262. Available from: http://stacks.iop.org/0022-3727/37/i=8/a=016. (Cited on page 33.)

Nieto-Vesperinas, M. (2006). *Scattering and Diffraction in Physical Optics*. World Scientific. (Cited on page 18.)

Nugent, K. A. (2009). Coherent methods in the x-ray sciences. *Advances in Physics*, 59(1):1–99. Available from: http://dx.doi.org/10.1080/00018730903270926, doi:10.1080/00018730903270926. (Cited on pages 8 and 9.)

Nye, J. F. (1999). *Natural Focusing and Fine Structure of Light: Caustics and Wave Dislocations*. Institute of Physics Publishing, Bristol. (Cited on page 64.)

Paganin, D., Mayo, S. C., Gureyev, T. E., Miller, P. R., and Wilkins, S. W. (2002). Simultaneous phase and amplitude extraction from a single defocused image of a homogeneous object. *Journal of Microscopy*, 206:33–40. (Cited on pages 71 and 72.)

Paganin, D. and Nugent, K. A. (1998a). Noninterferometric phase imaging with partially coherent light. *Physical Review Letters*, 80(12):2586–2589. Available from: http://link.aps.org/doi/10.1103/PhysRevLett.80.2586. (Cited on pages 9, 65, 66 and 83.)

Paganin, D. and Nugent, K. A. (1998b). Noninterferometric phase imaging with partially coherent light. *Physical Review Letters*, 80(12):2912. (Cited on page 43.)

Paganin, D. and Nugent, K. A. (2002). Phase measurement of waves that obey nonlinear equations. *Opt. Lett.*, 27(8):622–624. Available from: http://ol.osa.org/abstract.cfm?URI=ol-27-8-622. (Cited on pages 9, 63, 64 and 65.)

Paganin, D. M. (2006). *Coherent X-ray Optics*. Oxford University Press, New York. (Cited on pages 6, 7, 8, 9, 14, 20, 30, 31, 34, 37, 40, 43, 52, 59, 63, 65, 71, 72 and 79.)

Paganin, D. M., Gureyev, T. E., Mayo, S. C., Stevenson, A. W., Nesterets, Y. I., and Wilkins, S. W. (2004a). X-ray omni microscopy. *Journal of Microscopy*, 214(3):315–327. Available from: http://dx.doi.org/10.1111/j.0022-2720.2004.01315.x, doi:10.1111/j.0022-2720.2004.01315.x. (Cited on pages 71 and 85.)

Paganin, D. M., Gureyev, T. E., Pavlov, K. M., Lewis, R. A., and Kitchen, M. J. (2004b). Phase retrieval using coherent imaging system with linear transfer functions. *Optic Communications*, 234(1-6):87–105. (Cited on page 33.)

Pauli, W. (1933). Die allgemeinen Prinzipien der Wellenmechanik. *Handbuch der Physik*. (Cited on page 6.)

Pavlov, K. M., Gureyev, T. E., Paganin, D., Nesterets, Y. I., Morgan, M. J., and Lewis, R. A. (2004). Linear systems with slowly varying transfer functions and their application to x-ray phase-contrast imaging. *Journal of Physics D: Applied Physics*, 37(19):2746. Available from: http://stacks.iop.org/0022-3727/37/i=19/a=021. (Cited on page 32.)

Pavlov, K. M., Kewish, C. M., Davis, J. R., and Morgan, M. J. (2000). A new theoretical approach to x-ray diffraction tomography. *J. Phys. D Appl. Phys.*, 33(13):1596–1605. (Cited on page 11.)

Pavlov, K. M., Kewish, C. M., Davis, J. R., and Morgan, M. J. (2001). A variant on the geometrical optics approximation in diffraction enhanced tomography. *Journal of Physics D: Applied Physics*, 34(10A):A168. Available from: http://stacks.iop.org/0022-3727/34/i=10A/a=335. (Cited on page 50.)

Payne, L. E. and Weinberger, H. F. (1960). An optimal Poincaréinequality for convex domains. *Archive for rational machanics and analysis*, 5(1):286–292. Available from: http://dx.doi.org/10.1007/BF00252910, doi:10.1007/BF00252910. (Cited on page 73.)

Petersen, T. C., Keast, V. J., Johnson, K., and Duvall, S. (2007). Tem-based phase retrieval of p-n junction wafers using the transport of intensity equation. *Philosophical Magazine*, 87(24):3565–3578. Available from: http://www.tandfonline.com/doi/abs/10.1080/14786430701361388, doi:10.1080/14786430701361388. (Cited on pages 9, 43, 65 and 79.)

Pfeiffer, F., Bech, M., Bunk, O., Kraft, P., Eikenberry, E. F., Brönnimann, C., Grünzweig, C., and David, C. (2008). Hard-X-ray dark-field imaging using a grating interferometer. *Nature Materials*, 7(2):134–137. Available from: http://dx.doi.org/10.1038/nmat2096, doi:10.1038/nmat2096. (Cited on page 35.)

Pfeiffer, F., Kottler, C., Bunk, O., and David, C. (2007). Hard X-ray phase tomography with low-brilliance sources. *Physical Review Letters*, 98(10):108105–. Available from: http://link.aps.org/doi/10.1103/PhysRevLett.98.108105. (Cited on page 9.)

Pfeiffer, F., Weitkamp, T., Bunk, O., and David, C. (2006). Phase retrieval and differential phase-contrast imaging with low-brilliance x-ray sources. *Nature Physics*, 2:258 – 261. (Cited on page 35.)

Phatak, C., Beleggia, M., and De Graef, M. (2008). Vector field electron tomography of magnetic materials: Theoretical development. *Ultramicroscopy*, 108(6):503–513. Available from: http://www.sciencedirect.com/science/article/pii/S0304399107001957, doi:http://dx.doi.org/10.1016/j.ultramic.2007.08.002. (Cited on page 9.)

Phatak, C., Petford-Long, A. K., and De Graef, M. (2010). Three-dimensional study of the vector potential of magnetic structures. *Physical Review Letters*, 104(25):253901–. Available from: http://link.aps.org/doi/10.1103/PhysRevLett.104.253901. (Cited on page 9.)

Pinsker, Z. G. (1974). *Dinamicheskoe rasseianie rentgenovskikh luchei v idealnykh kristallakh*. Izd-vo "Nauka", Moskva. (Cited on pages 16, 31 and 32.)

Radon, J. (1917). Über die Bestimmung von Funktionen durch ihre Integralwerte längst gewisser Mannigfaltigkeiten. *Berichte Sächsische Akademie der Wissenschaften, Leipzig, Math.-Phys. Kl.*, 69:262–267. (Cited on page 44.)

Raven, C., Snigirev, A., Snigireva, I., Spanne, P., Souvorov, A., and Kohn, V. (1996). Phase-contrast microtomography with coherent high-energy synchrotron x rays. *Applied Physics Letters*, 69(13):1826–1828. Available from: http://dx.doi.org/10.1063/1.117446. (Cited on pages 9 and 50.)

Reed, M. and Simon, B. (1980). *Methods of Modern Mathematical Physics*. Academic, Orlando. (Cited on pages 52, 53 and 54.)

Rigon, L., Arfelli, F., and Menk, R.-H. (2007). Three-image diffraction enhanced imaging algorithm to extract absorption, refraction, and ultrasmall-angle scattering. *Applied Physics Letters*, 90(11):114102–3. Available from: http://dx.doi.org/10.1063/1.2713147. (Cited on pages 32 and 33.)

Saleh, B. E. A. and Teich, M. C. (2007). *Fundamentals of Photonics*. John Wiley & Sons, 2nd edition. (Cited on pages 63, 73 and 74.)

Sanner, C., Su, E. J., Keshet, A., Huang, W., Gillen, J., Gommers, R., and Ketterle, W. (2011). Speckle imaging of spin fluctuations in a strongly interacting fermi gas. *Physical Review Letters*, 106:010402. (Cited on pages 7 and 8.)

Schmalz, J. A., Gureyev, T. E., Paganin, D. M., and Pavlov, K. M. (2011). Phase retrieval using radiation and matter wave fields: Validity of Teague's method for solution of the transport of intensity equation. *Physical Review A*, 84(2):023808. (Cited on pages 6, 13, 61 and 83.)

Schmalz, J. A., Schmalz, G., Gureyev, T. E., and Pavlov, K. M. (2010). On the derivation of the Green's function for the Helmholtz equation using generalized functions. *American Journal of Physics*, 78(2):181–186. doi:10.1119/1.3253655. (Cited on pages 13, 17, 43 and 51.)

Schwartz, L. (1950-1951). *Théorie des distributions*, volume I-II. Paris. (Cited on page 52.)

Shabat, B. V. (1992). *Introduction to Complex Analysis*. R.I.American Mathematical Society, Providence. (Cited on page 56.)

Shi, D. and Anastasio, M. A. (2006). Off-axis holographic tomography for diffracting scalar wavefields. *Physical Review E*, 73(1):016612–. Available from: http://link.aps.org/doi/10.1103/PhysRevE.73.016612. (Cited on page 9.)

Snigirev, A., Snigireva, I., Kohn, V., Kouznetsov, S., and Schelokov, I. (1995). On the possibilities of x-ray phase contrast microimaging by coherent high-energy synchrotron radiation. *Review of Scientific Instruments*, 66:5486. (Cited on pages 10 and 50.)

Sobolev, S. (1936). Méthode nouvelle á résoudre le probléme de cauchy pour les équations linéaires hyperboliques normales. *Math.Sb.*, 1 (43):39–72. (Cited on page 52.)

Sommerfeld, A. (1949). *Partial Differential Equations in Physics*. Academic Press, New York. (Cited on pages 14 and 52.)

Spence, J. C. H. (2003). *Experimental High-Resolution Electron Microscopy*. Oxford University Press, New York, 3rd edition. (Cited on page 8.)

Sudarshan, E. C. G. (1980). Geometry of wave electromagnetics. *AIP Conference Proceedings*, 65(1):95–105. Available from: http://dx.doi.org/10.1063/1.32322. (Cited on page 66.)

Takeda, M., Ina, H., and Kobayashi, S. (1982). Fourier-transform method of fringe-pattern analysis for computer-based topography and interferometry. *J. Opt. Soc. Am.*, 72(1):156–160. (Cited on page 27.)

Talbot, H. F. (1836). On recent improvements in photography. *Philosophical Magazine*, 9:401. (Cited on page 34.)

Teague, R. M. (1983). Deterministic phase retrieval: a Green's function solution. *J. Opt. Soc. Am.*, 73(11):1434–1441. Available from: http://www.opticsinfobase.org/abstract.cfm?URI=josa-73-11-1434. (Cited on pages 9, 11, 13, 39, 41, 43, 64 and 83.)

Tikhonov, A. N. and Samarskii, A. A. (1990). *Equations of Mathematical Physics*. Dover, New York. (Cited on pages 65, 66, 67, 68, 69 and 71.)

Turner, L. D., Weber, K. P., Paganin, D., and Scholten, R. E. (2004). Off-resonant defocus-contrast imaging of cold atoms. *Optics Letters*, 29:232–234. (Cited on pages 7, 8 and 72.)

Vladimirov, V. (1971). *Equations of Mathematical Physics*. Marcel Dekker, New York. (Cited on pages 42, 52, 53, 54, 56, 57 and 121.)

Vladimirov, V. (1979). *Generalized Functions in Mathematical Physics*. Mir, Moscow. (Cited on pages 52, 53 and 54.)

Weitkamp, T., David, C., Kottler, C., Bunk, O., and Pfeiffer, F. (2006). Tomography with grating interferometers at low-brilliance sources. *Proc. SPIE*, pages 63180S–63180S. Available from: http://dx.doi.org/10.1117/12.683851. (Cited on page 50.)

Weitkamp, T., Diaz, A., David, C., Pfeiffer, F., Stampanoni, M., Cloetens, P., and Ziegler, E. (2005). X-ray phase imaging with a grating interferometer. *Opt. Express*, 13(16):6296–6304. Available from: http://www.opticsexpress.org/abstract.cfm?URI=oe-13-16-6296. (Cited on pages 34 and 35.)

Wernick, M. N., Wirjadi, O., D.Chapman, Zhong, Z., Galatsanos, N. P., Yang, Y., Brankov, J. G., Oltulu, O., Anastasio, M. A., and Muehleman, C. (2003). Multiple-image radiography. *Phys Med Biol*, 48(23):3875–95. (Cited on page 33.)

Wilkins, S. W., Gureyev, T. E., Gao, D., Pogany, A., and Stevenson, A. W. (1996). Phase-contrast imaging using polychromatic hard x-rays. *Nature (London)*, 384:335–338. (Cited on pages 7, 10 and 50.)

Wolf, E. (1969). Three-dimensional structure determination of semi-transparent objects from holographic data. *Opt. Commun.*, 1(4):153–156. (Cited on page 11.)

Wu, X. and Liu, H. (2004). A dual detector approach for x-ray attenuation and phase imaging. *Journal of X-Ray Science and Technology*, 12:35–42. (Cited on page 72.)

Wu, X., Liu, H., and Yan, A. (2005). X-ray phase-attenuation duality and phase retrieval. *Opt. Lett.*, 30(4):379–381. Available from: http://ol.osa.org/abstract.cfm?URI=ol-30-4-379. (Cited on page 85.)

X-ray complex refraction coefficients. CSIRO [online]. (2012). Available from: www.ts-imaging.net/Services/Simple/ICUtilXdata.aspx. (Cited on page 92.)

X-TRACT. CSIRO [online]. (2010). Available from: http://www.ts-imaging.net/Services/AppInfo/X-TRACT.aspx. (Cited on pages 77 and 90.)

Yu, R. P., Morgan, M. J., and Paganin, D. M. (2011). Lorentz-electron vector tomography using two and three orthogonal tilt series. *Physical Review A*, 83:023813. (Cited on pages 8, 9, 43 and 65.)

Yu, R. P., Paganin, D. M., and Morgan, M. J. (2005). Inferring nonlinear parabolic field equations from modulus data. *Physics Letters A*, 341:156–163. (Cited on pages 6, 43, 65 and 79.)

Yu, X. Z., Onose, Y., Kanazawa, N., Park, J. H., Han, J. H., Marsui, Y., Nagaosa, N., and Tokura, Y. (2010). Real-space observation of a two-dimensional skyrmion crystal. *Nature (London)*, 465:901–904. (Cited on pages 9, 43, 65 and 79.)

Zernike, v. F. (1934). Beugungstheorie des Schneidenver-Fahrens und seiner verbesserten Form, der phasenkontrastmethode. *Physica*, 1(7–12):689–704. Available from: http://www.sciencedirect.com/science/article/pii/S0031891434802595, doi:http://dx.doi.org/10.1016/S0031-8914(34)80259-5. (Cited on page 42.)

Zhou, S.-A. and Brahme, A. (2008). Development of phase-contrast x-ray imaging techniques and potential medical applications. *Physica Medica*, 24(3):129–148. Available from: http://www.sciencedirect.com/science/article/pii/S1120179708000689, doi:http://dx.doi.org/10.1016/j.ejmp.2008.05.006. (Cited on page 8.)

Appendix

A Definition and Properties of the Fourier Transform

The forward and inverse Fourier transforms in the 1D, 2D and 3D are defined as follows:

$$\mathbf{F_1}[f](\xi) = \int_{-\infty}^{\infty} e^{-2\pi i x \xi} f(x) dx, \tag{A.1}$$

$$\mathbf{F_1}^{-1}[\hat{f}](x) = \int_{-\infty}^{\infty} e^{2\pi i x \xi} \hat{f}(\xi) d\xi, \tag{A.2}$$

$$\mathbf{F_2}[f](\xi, \eta) = \iint_{-\infty}^{\infty} e^{-2\pi i (x\xi + y\eta)} f(x, y)\, dx dy, \tag{A.3}$$

$$\mathbf{F_2}^{-1}[\hat{f}](x, y) = \iint_{-\infty}^{\infty} e^{2\pi i (x\xi + y\eta)} \hat{f}(\xi, \eta)\, d\xi d\eta, \tag{A.4}$$

$$\mathbf{F}_3[f](\xi, \eta, \zeta) = \iiint_{-\infty}^{\infty} e^{-2\pi i (x\xi + y\eta + z\zeta)} f(x, y, z)\, dx dy dz, \tag{A.5}$$

$$\mathbf{F_3}^{-1}[\hat{f}](x, y, z) = \iiint_{-\infty}^{\infty} e^{2\pi i (x\xi + y\eta + z\zeta)} \hat{f}(\xi, \eta, \zeta)\, d\xi d\eta d\zeta, \tag{A.6}$$

where ξ, η, and ζ are the dual coordinates in the Fourier space to x, y and z, respectively.

We use the following properties of the one-dimensional ($n = 1$), two-dimensional ($n = 2$) and three-dimensional ($n = 3$) Fourier transform:

(i) linearity, i.e.

$$\mathbf{F}_n[af + bg] = a\mathbf{F}_n[f] + b\mathbf{F}_n[g], \tag{A.7}$$

where a and b are constants,

(ii) invertibility, i.e.

$$\mathbf{F}_n^{-1}[\mathbf{F}_n[f]] = f, \tag{A.8}$$

(iii) Fourier transform of derivative

$$\mathbf{F}_n\left[\frac{\partial}{\partial x} f\right] = 2\pi i \xi \mathbf{F}_n[f]. \tag{A.9}$$

B Solutions of the homogeneous Helmholtz equation

We solve the following equation in the space of generalized functions (i.e. distributions):

$$(\xi^2 + \eta^2 + \zeta^2 - \rho^2)\hat{G}_{\text{hom}} = 0, \tag{B.10}$$

where $\rho = k/2\pi$ and $\hat{G}_{\text{hom}}$ is a generalised function in three-dimensional space. We will show that the solutions are the simple layers $\mu\delta_S$ on the Ewald sphere S: $\xi^2 + \eta^2 + \zeta^2 - \rho^2 = 0$ that act on the test functions φ by $\langle \mu, \varphi|_S \rangle$ (Equation (7.4)), where $\varphi|_S$ is the restriction of φ on S.

First we show that $\mu\delta_S$ is a solution of the equation. In fact,

$$\langle (\xi^2 + \eta^2 + \zeta^2 - \rho^2)\mu\delta, \varphi \rangle = \langle \mu\delta, (\xi^2 + \eta^2 + \zeta^2 - \rho^2)\varphi \rangle \tag{B.11a}$$

$$= \langle \mu, [(\xi^2 + \eta^2 + \zeta^2 - \rho^2)\varphi]|_S \rangle \tag{B.11b}$$

$$= \langle \mu, 0 \rangle = 0. \tag{B.11c}$$

We have used the definition of multiplication of generalised functions (see for example, Ref.(Vladimirov, 1971, Section 2.5.9)) and the definition of a simple layer.

We now show that there are no other solutions. Let $\hat{G}_{\text{hom}}$ be a solution. To construct the corresponding μ we introduce a smooth function $\chi(\xi,\eta,\zeta)$ with compact support that vanishes on some neighbourhood of 0 and is identically 1 on S. For a solution $\hat{G}_{\text{hom}}$ we define a generalised function μ on S by

$$\langle \mu, \psi \rangle = \langle \hat{G}_{\text{hom}}, \chi\psi^* \rangle, \tag{B.12}$$

where ψ^* is the radial extension of ψ; that is, $\psi^*(\xi,\eta,\zeta) = \psi(\rho\frac{\xi}{\kappa}, \rho\frac{\eta}{\kappa}, \rho\frac{\zeta}{\kappa})$, where $\kappa = \sqrt{\xi^2+\eta^2+\zeta^2} \neq 0$ and $\psi^*(0,0,0) = 0$. We show that $\mu\delta_S = \hat{G}_{\text{hom}}$ using that any test function φ decomposes into $\varphi = \chi(\varphi|_S)^* + \varphi_1$, where $\varphi_1 = 0$ on S and is therefore divisible by $\xi^2+\eta^2+\zeta^2-\rho^2$; that is, $\varphi_1 = (\xi^2+\eta^2+\zeta^2-\rho^2)\varphi_2$.

It follows that

$$\langle \hat{G}_{\text{hom}}, \varphi \rangle = \langle \hat{G}_{\text{hom}}, \chi(\varphi|_S)^* + (\xi^2+\eta^2+\zeta^2-\rho^2)\varphi_2 \rangle \tag{B.13a}$$

$$= \langle \hat{G}_{\text{hom}}, \chi(\varphi|_S)^* \rangle = \langle \mu, \varphi|_S \rangle, \tag{B.13b}$$

as required. Here we used that $\hat{G}_{\text{hom}}$ is a solution of Equation (B.10) and hence $\langle \hat{G}_{\text{hom}}, (\xi^2+\eta^2+\zeta^2-\rho^2)\varphi_2 \rangle = 0$. The last equality is a consequence of the definition (B.12) of μ.

C Rotational symmetry and the Fourier transform

We show that the Fourier image is rotationally symmetric if the original function is also rotationally symmetric. Assume $G(\mathbf{r})$ with $\mathbf{r} = (x,y,z)$ is rotationally invariant; that is, $G(A\mathbf{r}) = G(\mathbf{r})$ for all orthogonal matrices A. Then

$$\hat{G}(A\boldsymbol{\kappa}) = \iiint e^{-2\pi i A\boldsymbol{\kappa}\cdot\mathbf{r}} G(\mathbf{r})\,dx\,dy\,dz, \tag{C.1}$$

where $\boldsymbol{\kappa} = (\xi,\eta,\zeta)$. The coordinate change $\mathbf{r} = A\mathbf{r}'$ transforms the integral on the right-hand side into

$$\iiint e^{-2\pi i A\boldsymbol{\kappa}\cdot A\mathbf{r}'} G(A\mathbf{r}')\,dx\,dy\,dz. \tag{C.2}$$

Note that an orthogonal transformation does not change the volume element. From the orthogonality of A we obtain $A\boldsymbol{\kappa}\cdot A\mathbf{r}' = \boldsymbol{\kappa}\cdot\mathbf{r}'$, and hence

$$\hat{G}(A\boldsymbol{\kappa}) = \iiint e^{-2\pi i\boldsymbol{\kappa}\cdot\mathbf{r}'} G(A\mathbf{r}')\,dx\,dy\,dz. \tag{C.3}$$

Now, $G(A\mathbf{r}') = G(\mathbf{r}')$ implies that the right-hand side equals

$$\iiint e^{-2\pi i \boldsymbol{\kappa}\cdot\mathbf{r}'} G(\mathbf{r}')\, dx\,dy\,dz = \hat{G}(\boldsymbol{\kappa}) \tag{C.4}$$

as required.

D Rotationally invariant generalised functions on the sphere

Here we prove that the only rotationally invariant generalised function G on the sphere S is a constant simple layer; that is, $G = \mu\delta_S$, where the density μ is a constant.

By definition, G is said to be rotationally invariant if

$$\langle G, \varphi \circ A\rangle = \langle G, \varphi\rangle \tag{D.1}$$

for all test functions φ and for all orthogonal matrices A. Here $\varphi \circ A$ is the composition of φ and A.

We prove the invariance for generalised functions by averaging the test functions over the group SO(3) of orthogonal matrices. Any matrix of SO(3) can be represented as a product of

$$\begin{pmatrix} \cos\alpha\cos\beta & -\sin\alpha & -\cos\alpha\sin\beta \\ \sin\alpha\cos\beta & \cos\alpha & -\sin\alpha\sin\beta \\ \sin\beta & 0 & \cos\beta \end{pmatrix} \begin{pmatrix} 1 & 0 & 0 \\ 0 & \cos\gamma & -\sin\gamma \\ 0 & \sin\gamma & \cos\gamma \end{pmatrix}, \tag{D.2}$$

where $\alpha \in (-\pi, \pi]$, $\beta \in [-\frac{\pi}{2}, \frac{\pi}{2}]$, and $\gamma \in (-\pi, \pi]$ are the Euler angles (see for example, Ref. (Goldshtein, 1980, Ch. 4.6)). The first column of the first factor represents a point of the unit sphere S_2, and the second factor represents a point of the unit circle S_1. Integration over SO(3) can be reduced to an iterated integral over the circle S_1 first and then over the sphere S_2 (see Ref. (Natterer, 2001, Ch. VII.2)). Then for any test function φ on S_2 we have

$$\iiint_{SO(3)} \varphi \circ A\, dV = \iint_{S_2} \left(\int_{S_1} \varphi(\mathbf{r})\, ds \right) dS = \iint_{S_2} \varphi(\mathbf{r})\, dS, \tag{D.3}$$

where dV, ds, dS are the invariant volume, length and area elements on SO(3), S_1 and S_2 respectively.

Let G be a rotationally invariant generalised function on S_2. Then

$$\langle G, \varphi\rangle = \iiint_{A\in SO(3)} \langle G, \varphi\circ A\rangle dV = \left\langle G, \iiint_{SO(3)} \varphi \circ A\, dV \right\rangle = \iint_{S_2} \varphi(\mathbf{r}) dS\, \langle G, 1\rangle.$$

(D.4)

The last expression is the integral of the test function over the sphere times the constant $\mu = \langle G, 1\rangle$, that is, a simple layer with constant density. We used linearity and continuity of G to change the order of integration and application of G and Equation (D.3).

E Lemmata for Chapter 9

Lemma 1 *For any function* $f(x, y, z)$ *from the Schwarz space*

$$\mathbf{F_3}\left[\nabla^2 f\right](\xi' \sin\theta, \eta, \xi' \cos\theta) = -4\pi^2(\xi'^2 + \eta^2)\mathbf{F_3}\left[f\right](\xi' \sin\theta, \eta, \xi' \cos\theta) \quad \text{(E.1)}$$

Proof: We use the property (Equation (A.9)) of the Fourier transform for this calculations:

$$\begin{aligned}&\mathbf{F_3}\left[\nabla^2 f\right](\xi' \sin\theta, \eta, \xi' \cos\theta) = \\ &-4\pi^2\left(\xi' \sin\theta^2 + \eta^2 + \xi' \cos\theta^2\right)\mathbf{F_3}\left[f\right](\xi' \sin\theta, \eta, \xi' \cos\theta) = \\ &\qquad -4\pi^2(\xi'^2 + \eta^2)\mathbf{F_3}\left[f\right](\xi' \sin\theta, \eta, \xi' \cos\theta). \quad \text{(E.2)}\end{aligned}$$

Lemma 2 *For any* $f(x, y, z)$ *from the Schwarz space*

$$\nabla_\perp^2\left(Pf\right)(x, y) = P\left(\nabla^2 f(x, y, z)\right) \quad \text{(E.3)}$$

Proof: Apply the slice theorem to Laplacian $\nabla^2 f(x, y, z)$ (for the plane $\theta = 0$)

$$\mathbf{F_2}\left[P\left(\nabla^2 f\right)\right](\xi', \eta) = \mathbf{F_3}\left[\nabla^2 f\right](0, \eta, \xi'). \quad \text{(E.4)}$$

Apply Lemma 1 to the right hand side and get

$$\mathbf{F_3}\left[\nabla^2 f\right](0, \eta, \xi') = -4\pi^2(\xi'^2 + \eta^2)\mathbf{F_3}\left[f\right](0, \eta, \xi'). \quad \text{(E.5)}$$

Apply the slice theorem to obtain

$$-4\pi^2(\xi'^2 + \eta^2)\mathbf{F_3}\left[f\right](0, \eta, \xi') = -4\pi^2(\xi'^2 + \eta^2)\mathbf{F_2}[Pf](\xi', \theta). \quad \text{(E.6)}$$

Using one of the properties of the Fourier transform (Equation (A.9)) we rewrite the last equation as

$$-4\pi^2(\xi'^2 + \eta^2)\mathbf{F_3}[Pf](\xi', \eta) = \mathbf{F_2}\left[\nabla_\perp^2 Pf\right](\xi', \eta). \quad \text{(E.7)}$$

We have shown that

$$\mathsf{F_2}\left[\mathsf{P}\left(\nabla^2 \mathsf{f}\right)\right](\xi', \eta) = \mathsf{F_2}\left[\nabla_\perp^2 \mathsf{P}\mathsf{f}\right](\xi', \eta), \tag{E.8}$$

it follows that

$$\mathsf{P}\left(\nabla^2 \mathsf{f}\right) = \nabla_\perp^2 \mathsf{P}(\mathsf{f}). \tag{E.9}$$

(property of the Fourier transform Equation (A.9))